Article

The Research on Harmonic Transfer Characteristics of Integrated Multi-Winding Inductive Filtering Converter Transformer and Its Filter System

Jianying Li [1,2,*], Yunchang Xiao [1,2], Minsheng Yang [1,2], Jianqi Li [1,2] and Jingying Wan [1,2]

[1] School of Computer and Electrical Engineering, Hunan University of Arts and Science, Changde 415000, China; xyc2961@huas.edu.cn (Y.X.); yms1234@huas.edu.cn (M.Y.); li_jianqi@126.com (J.L.); wan_jy@huas.edu.cn (J.W.)

[2] Key Laboratory of Hunan Province for Control Technology of Distributed Electric Propulsion Air Vehicle, Changde 415000, China

* Correspondence: ljymnn@huas.edu.cn

Abstract: A novel integrated multi-winding inductive filter converter and its filter system used in HVDC conversion station are proposed. Specifically, the schemes include two paralleled-connected delta filter windings with zero impedance, and the 11th and 13th tuned filtering branches are installed at the taps. On this basis, the 5th and 7th harmonic filters are eliminated and the 5th, 7th, 11th, and 13th harmonics of the valve-side are suppressed. Moreover, the cost of the filter is reduced, and the negative impact on the converter transformer body caused by the transfer of harmonic current is avoided, such as vibration, noise, and harmonic loss. In this paper, first, the mathematical models of integrated multi-winding inductive filter converter and its filter system are established. Accordingly, the current relationships between the primary winding side and two secondary winding sides are derived. Then, the transfer path of each characteristic harmonic current in the new system is analyzed and discussed. Moreover, a simulation model is established to study the operation characteristics of the system. Finally, through the designed experimental prototype, a new DC transferring system platform is constructed to testify the operation characteristics of an integrated multi-winding inductive filter converter and its filter system. The experimental results show that the total harmonic distortion rate of the grid-winding current can be reduced to 4.68% only by installing the 11th and 13th tuned filters, so the effect of active filtering is approximated realized by the passive filtering method.

Keywords: inductive filtering converter transformer; harmonic suppression; operation characteristics; harmonic transfer paths

1. Introduction

The traditional 12-pulse converter system is a parallel topology composed of two parts, in which each part has two transformers with a 6-pulse converter bridge and the transformers are connected by Y-Y and Y-Δ structure, respectively. The orders of characteristic harmonics generated by the upper and lower bridge converter valves in the commutation process are $6n \pm 1$ (n is a positive integer). Therefore, the 5th, 7th, 11th, and 13th harmonics are the main ones [1–4]. When the two sets of windings of the upper and lower bridge converter transformer have a phase difference of 30° and the winding turn ratio is 1:$\sqrt{3}$, the generated $12n - 5, 12n - 7$-th (n is a positive integer) harmonics of bridge converter valves are offset by the phase-shifting confluence on the grid-side. In this way, the grid-side current of the 12 pulse converter system only contains $12n \pm 1$-th (n is a positive integer) characteristic harmonics [5–11], in which the 11th and 13th harmonic currents can be filtered by the corresponding harmonic filters installed on the AC side. Thus, when the harmonic current is transferred in the converter transformer, the negative impact on the converter transformer,

such as vibration, noise, and harmonic loss, still exists [12–15]. In contrast, the inductive filter converter transformer has a special integrated filter winding that uses zero impedance, which can suppress harmonics on the valve-side with the corresponding tuned filter device [16–24]. In Ref. [25], scholars analyzed the operation characteristics of an inductive filter rectifier transformer, and its filter system applied to the industrial rectifier system. In this study, the 5th, 7th, 11th, and 13th harmonics could be suppressed by connecting the corresponding tuned filters on the special integrated delta filter winding. Based on this, the 6-pulse rectifier unit could form multiple rectifier systems with different typologies, such as a 12-pulse rectifier system, but the installation of two sets of tuned filters with the order of 5, 7, 11, and 13 will increase the volume and cost of the filter. Nevertheless, these researchers have provided a theoretical basis for this paper.

A novel 12-pulse inductive filter converter transformer with parallel topology of two delta filter windings is proposed for an HVDC conversion station in this paper, and it is called an integrated multi-winding inductive filtering converter transformer here. Specifically, the two delta windings designed with zero impedance are parallel-connected to eliminate the 5th and 7th harmonic filters, while suppressing the harmonics on the valve-side. Moreover, it is only necessary to install a set of 11th and 13th tuned filtering branches at the taps to achieve the desired filtering performance. These measures greatly simplify design and reduce the cost of the filter. The harmonic suppression method proposed in this paper can prevent the harmonic currents generated by the rectifier from flowing into the grid side winding of the new transformer using a unique zero equivalent impedance design. The negative effects of the harmonic currents on the converter transformer, such as harmonic losses, heat, noise, vibration, etc., are therefore greatly reduced, so as to the effect of active filtering is approximated realized by the passive filtering method.

In this paper, an influence of the parallel-connected two delta windings designed with zero impedance on the harmonic transfer characteristics is analyzed, as well as the transfer path of each harmonic current. First, the mathematical models of new inductive filter converter and its filter system are established. Then, the current relationships between different windings are conducted, and the harmonic current paths and reactive power compensation characteristics of this new system are demonstrated. Next, the operation characteristics of the new system are simulated by software. Moreover, the experimental prototype is designed according to integrated multi-winding inductive filter converter and its filter system, to verify the correctness of the system.

2. Wiring Scheme of the Integrated Multi-Winding Inductive Filter Converter Transformer and Its Filter System

Figure 1 shows the wiring scheme of the integrated multi-winding inductive filter converter transformer and its filter system, which includes two paralleled-connected delta filter windings.

The iron core of the integrated multi-winding inductive filter converter transformer adopts the single-phase dual-column yoke-type structure. There are three windings on the left and right core columns, which are grid-side winding, valve-side winding, and filter-side winding, respectively. Two sets of grid-side windings are connected in parallel, using star connection. Among the two sets of valve-side windings, the upper winding of the left column is connected with the upper bridge converter valve by star connection, and the upper winding of the right column is connected with the lower bridge converter valve by the delta structure. Two sets of filter windings are connected in parallel, and the filters in them are connected by the delta structure. The turn number of two grid-side windings of the proposed inductive filter converter transformer is W_1 The turn number of the valve-side winding of upper bridge with a star connection is W_2. The turn number of the valve-side winding of lower bridge with a delta connection is W_3. The turn number of both sets of filter-side windings is W_L. To realize the uniform distribution of the load current between windings on the valve-side and good operation of the 12-pulse converter system, the turns of the delta-connected winding on the valve-side are $\sqrt{3}$ times that of

the star-connected winding on the valve-side. The winding parameters of the left and right core columns of the converter transformer are completely symmetrical. Therefore, the short-circuit impedance parameters between the grid-side winding and the valve-side winding of the left and right columns are consistent, expressed by Z_{k12}. The short-circuit impedance parameters between the grid-side winding and the filter-side winding of the left and right columns are Z_{k13}. The short-circuit impedance parameters between the valve-side winding and the filter-side winding on the left and right columns are represented by Z_{k23}.
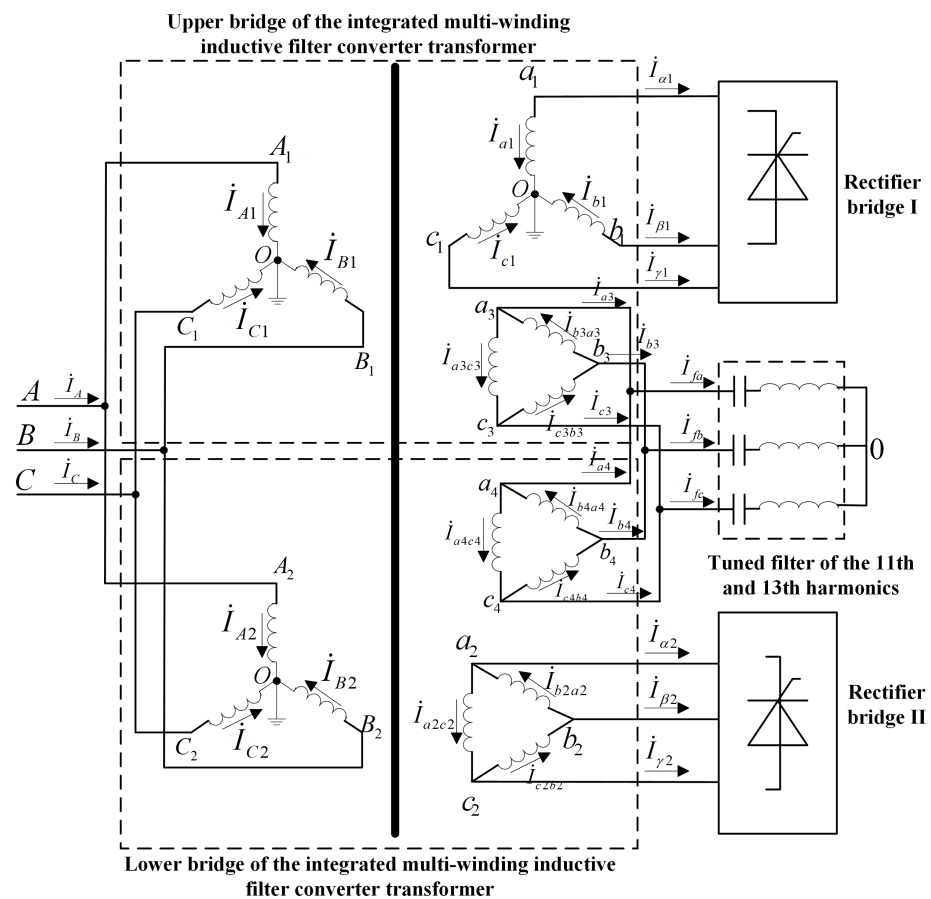
Figure 1. Wiring scheme of the integrated multi-winding inductive filter converter transformer and its filter system.

3. Mathematical Model of the Integrated Multi-Winding Inductive Filter Converter Transformer and Its Filter System

The following assumptions should be made before building the mathematical model. It is assumed that the three-phase symmetry of the AC system is an ideal sine wave with the same frequency. The parameters of the upper and lower bridge converter valves are assumed to be completely symmetrical. It is assumed that the parameters of the winding at left and right column of the converter transformer are completely symmetrical. Based on the above assumptions, the winding magnetic potentials on the left and right column are independent of each other, and the electromagnetic relationship between the upper and lower bridge converter transformers can be discussed separately.

3.1. Mathematical Model of the Upper Bridge Converter Transformer and Its Filter System

Combining the wiring scheme in Figure 1 with the theory of multi-winding transformer [26], the voltage transfer equations for the single-phase winding of the upper bridge converter transformer are as follows:

$$
\begin{cases}
\dot{U}_{AO} - \frac{W_1}{W_2}\dot{U}_{a1o} = -\frac{W_2}{W_1}\dot{I}_{a1}Z_{k12} - \frac{W_L}{W_1}\dot{I}_{a3c3}Z_1 \\
\dot{U}_{AO} - \frac{W_1}{W_L}\dot{U}_{a3c3} = -\frac{W_2}{W_1}\dot{I}_{a1}Z_1 - \frac{W_L}{W_1}\dot{I}_{a3c3}Z_{k13}.
\end{cases}
\tag{1}
$$

Among them, W_1, W_2, and W_L are the turn numbers of windings at grid-side, valve-side, and filter, respectively. Z_1 is the equivalent impedance of winding at grid-side. Z_{k12} is the short-circuit impedance between windings of a grid-side and valve-side of the upper bridge. Z_{k13} is the short-circuit impedance between windings of the grid-side and filter-side.

Ignoring the excitation current of transformer core and according to the principle of magnetic potential balance, the magnetic potential balance equation of winding at the upper bridge inductive filter converter transformer can be obtained as follows:

$$
\dot{I}_{A1} + \frac{W_2}{W_1}\dot{I}_{a1} + \frac{W_L}{W_1}\dot{I}_{a3c3} = 0
\tag{2}
$$

According to Figure 1, the following equation can be obtained according to KVL and KCl laws:

$$
\begin{cases}
\dot{U}_{a3c3} = \left(\dot{I}_{fa} - \dot{I}_{fc}\right)Z_f = \sqrt{3}e^{-j30°}Z_f\dot{I}_{fa} \\
\dot{I}_{\alpha1} = -\dot{I}_{a1}
\end{cases}
\tag{3}
$$

where Z_f is the fundamental frequency impedance of the tuned filter.

Substituting Equations (2) and (1) into Equation (3), there is

$$
\dot{U}_{AO} - \frac{\sqrt{3}W_1}{W_L}e^{-j30°}Z_f\dot{I}_{fa} = \frac{W_2}{W_1}Z_1\dot{I}_{\alpha1} - \frac{(W_L^2 Z_1 + W_1^2 Z_3)}{W_1 W_L}\dot{I}_{a3c3}
\tag{4}
$$

3.2. Mathematical Model of Lower Bridge Converter Transformer and Its Filtering System

Combining the wiring scheme of an integrated multi-winding inductive filter converter transformer and its filter system in Figure 1 with the theory of a multi-winding transformer [26], the voltage transfer equations of the single-phase winding of the lower bridge converter transformer are

$$
\begin{cases}
\dot{U}_{AO} - \frac{W_1}{W_3}\dot{U}_{a2c2} = -\frac{W_3}{W_1}\dot{I}_{a2c2}Z_{k12} - \frac{W_L}{W_1}\dot{I}_{a4c4}Z_1 \\
\dot{U}_{AO} - \frac{W_1}{W_L}\dot{U}_{a4c4} = -\frac{W_3}{W_1}\dot{I}_{a2c2}Z_1 - \frac{W_L}{W_1}\dot{I}_{a4c4}Z_{k13}
\end{cases}
\tag{5}
$$

where W_1, W_3, and W_L are the turn numbers of windings at grid-side, valve-side, and filter, respectively. Z_1 is the equivalent impedance of winding at grid-side. Z_{k12} is the short-circuit impedance between windings of grid-side and valve-side of the lower bridge. Z_k13 is the short-circuit impedance windings of the grid-side and filter-side.

When ignoring the excitation current of the transformer core, the magnetic potential balance equation of winding at the lower bridge inductive filter converter transformer can be obtained as presented in Equation (6) according to the principle of magnetic potential balance:

$$
\dot{I}_{A2} + \frac{W_3}{W_1}\dot{I}_{a2c2} + \frac{W_L}{W_1}\dot{I}_{a4c4} = 0
\tag{6}
$$

According to Figure 1, the following equation can be obtained according to KVL and KCl laws:

$$
\begin{cases}
\dot{U}_{a4c4} = \left(\dot{I}_{fa} - \dot{I}_{fc}\right)Z_f = \sqrt{3}e^{-j30°}Z_f\dot{I}_{fa} \\
\dot{I}_{\alpha2} = \dot{I}_{b2a2} - \dot{I}_{a2c2} = -\sqrt{3}e^{j30°}\dot{I}_{a2c2}
\end{cases}
\tag{7}
$$

where Z_f is the fundamental frequency impedance of the tuned filter.

Substituting Equations (6) and (7) into Equation (5), there is

$$\dot{U}_{AO} - \frac{\sqrt{3}W_1}{W_L}e^{-j30°}Z_f\dot{I}_{fa} = \frac{W_3}{\sqrt{3}W_1}Z_1e^{-j30°}\dot{I}_{\alpha2} - \frac{(W_L^2Z_1 + W_1^2Z_3)}{W_1W_L}\dot{I}_{a4c4} \tag{8}$$

3.3. Unified Mathematical Models of Bridge Converter Transformers and Their Filter Systems

The current equations flowing into the filter on the filter-side can be obtained from Figure 1 as

$$\begin{cases} \dot{I}_{a3} = -\sqrt{3}e^{j30°}\dot{I}_{a3c3} \\ \dot{I}_{a4} = -\sqrt{3}e^{j30°}\dot{I}_{a4c4} \\ \dot{I}_{fa} = \dot{I}_{a3} + \dot{I}_{a4} = -\sqrt{3}e^{j30°}\left(\dot{I}_{a3c3} + \dot{I}_{a4c4}\right) \end{cases} \tag{9}$$

In the integrated multi-winding inductive filter converter transformer, note that the turn number of the star-connected winding at the valve-side of the upper bridge is W_2, and the turn number of the delta-connected winding at valve-side of the lower bridge is W_3. Both satisfy the following equation:

$$\frac{W_3}{W_2} = \sqrt{3} \tag{10}$$

Combining Equations (4) and (8)–(10), the current equation of valve-side and filter-side can be obtained as

$$\begin{aligned} \dot{I}_{fa} &= \frac{2\sqrt{3}W_1W_Le^{j30°}}{W_L^2Z_1 + W_1^2Z_3 + 6W_1^2Z_f}\dot{U}_{AO} - \frac{\sqrt{3}W_2W_LZ_1e^{j30°}}{W_L^2Z_1 + W_1^2Z_3 + 6W_1^2Z_f}\left(\dot{I}_{\alpha1} + e^{-j30°}\dot{I}_{\alpha2}\right) \\ &= \frac{2\sqrt{3}W_1W_Le^{j30°}}{\lambda}\dot{U}_{AO} - \frac{\sqrt{3}W_2W_LZ_1e^{j30°}}{\lambda}\left(\dot{I}_{\alpha1} + e^{-j30°}\dot{I}_{\alpha2}\right) \end{aligned} \tag{11}$$

wherein $\lambda = W_L^2Z_1 + W_1^2Z_3 + 6W_1^2Z_f$.

Substituting Equations (11), (3), and (2) into (1), the winding current equation at the grid-side and valve-side of the upper bridge can be obtained as follows:

$$\dot{I}_{A1} = \frac{W_L^2}{\lambda}\dot{U}_{AO} + \frac{3W_1W_2W_L^2Z_fZ_1 + Z_3W_1W_2\lambda}{\lambda(W_L^2Z_1 + W_1^2Z_3)}\dot{I}_{\alpha1} + \frac{3W_1W_2W_L^2Z_fZ_1}{\lambda(W_L^2Z_1 + W_1^2Z_3)}e^{-j30°}\dot{I}_{\alpha2} \tag{12}$$

Similarly, by substituting Equations (11), (7), and (6) into (5), the winding current equation at the grid-side and valve-side of the lower bridge can also be obtained:

$$\dot{I}_{A2} = \frac{W_L^2}{\lambda}\dot{U}_{AO} + \frac{3W_1W_2W_L^2Z_fZ_1}{\lambda(W_L^2Z_1 + W_1^2Z_3)}\dot{I}_{\alpha1} + \frac{3W_1W_2W_L^2Z_fZ_1 + Z_3W_1W_2\lambda}{\lambda(W_L^2Z_1 + W_1^2Z_3)}e^{-j30°}\dot{I}_{\alpha2} \tag{13}$$

The current equations of the filter-side winding of the upper and lower bridges are

$$\dot{I}_{a3} = \frac{\sqrt{3}W_1W_Le^{j30°}}{\lambda}\dot{U}_{AO} - \frac{\sqrt{3}W_2W_LZ_1\left(W_L^2Z_1 + W_1^2Z_3 + 3W_1^2Z_f\right)}{\lambda(W_L^2Z_1 + W_1^2Z_3)}e^{j30°}\dot{I}_{\alpha1} + \frac{3\sqrt{3}W_1^2W_2W_LZ_fZ_1}{\lambda(W_L^2Z_1 + W_1^2Z_3)}\dot{I}_{\alpha2} \tag{14}$$

$$\dot{I}_{a4} = \frac{\sqrt{3}W_1W_Le^{j30°}}{\lambda}\dot{U}_{AO} + \frac{3\sqrt{3}W_1^2W_2W_LZ_fZ_1}{\lambda(W_L^2Z_1 + W_1^2Z_3)}e^{j30°}\dot{I}_{\alpha1} - \frac{\sqrt{3}W_2W_LZ_1\left(W_L^2Z_1 + W_1^2Z_3 + 3W_1^2Z_f\right)}{\lambda(W_L^2Z_1 + W_1^2Z_3)}\dot{I}_{\alpha2} \tag{15}$$

4. Transfer Characteristics of Harmonics in an Integrated Multi-Winding Inductive Filter Converter Transformer and Its Filter System

Assuming that the power supply connected to the winding on grid-side of the transformer is an ideal voltage source and does not contain any harmonic, then the converter valve connected to the winding on the valve-side can be treated as a harmonic current source, that is:

$$\dot{U}_{AO}^{(h)} = 0 \tag{16}$$

To analyze the influence of the parallel topology structure of two delta filter windings adopted by the integrated multi-winding inductive filter converter transformer on the harmonic transfer characteristics of the system, the established Equations (12) and (13) are also adopted. Accordingly, the harmonic characteristic equations of the grid-side winding and valve-side winding of the proposed filter converter transformer can be obtained by combining Equation (16), as shown in Equation (17):

$$
\begin{cases}
\dot{I}_{A1}^{(h)} = \frac{3W_1 W_2 W_L^2 Z_f^{(h)} Z_1^{(h)} + Z_3^{(h)} W_1 W_2 \lambda^{(h)}}{\lambda^{(h)} \left(W_L^2 Z_1^{(h)} + W_1^2 Z_3^{(h)} \right)} \dot{I}_{\alpha1}^{(h)} + \frac{3W_1 W_2 W_L^2 Z_f^{(h)} Z_1^{(h)}}{\lambda^{(h)} \left(W_L^2 Z_1^{(h)} + W_1^2 Z_3^{(h)} \right)} e^{-j30°} \dot{I}_{\alpha2}^{(h)} \\[3mm]
\dot{I}_{A2}^{(h)} = \frac{3W_1 W_2 W_L^2 Z_f^{(h)} Z_1^{(h)}}{\lambda^{(h)} \left(W_L^2 Z_1^{(h)} + W_1^2 Z_3^{(h)} \right)} \dot{I}_{\alpha1}^{(h)} + \frac{3W_1 W_2 W_L^2 Z_f^{(h)} Z_1^{(h)} + Z_3^{(h)} W_1 W_2 \lambda^{(h)}}{\lambda^{(h)} \left(W_L^2 Z_1^{(h)} + W_1^2 Z_3^{(h)} \right)} e^{-j30°} \dot{I}_{\alpha2}^{(h)}
\end{cases}
\tag{17}
$$

Among them, $\lambda^{(h)} = W_L^2 Z_1^{(h)} + W_1^2 Z_3^{(h)} + 6W_1^2 Z_f^{(h)}$, and h is the order of harmonic, $h = 5, 7, 11, 13, 17, 19\ldots$

According to Equations (11) and (14)–(16), the harmonic characteristic equations of valve-side winding and filter-side winding can be obtained as

$$
\begin{cases}
\dot{I}_{a3}^{(h)} = -\frac{\sqrt{3} W_2 W_L Z_1^{(h)} \left(W_L^2 Z_1^{(h)} + W_1^2 Z_3^{(h)} + 3W_1^2 Z_f^{(h)} \right)}{\lambda^{(h)} \left(W_L^2 Z_1^{(h)} + W_1^2 Z_3^{(h)} \right)} e^{j30°} \dot{I}_{\alpha1}^{(h)} + \frac{3\sqrt{3} W_1^2 W_2 W_L Z_f^{(h)} Z_1^{(h)}}{\lambda^{(h)} \left(W_L^2 Z_1^{(h)} + W_1^2 Z_3^{(h)} \right)} \dot{I}_{\alpha2}^{(h)} \\[3mm]
\dot{I}_{a4}^{(h)} = \frac{3\sqrt{3} W_1^2 W_2 W_L Z_f^{(h)} Z_1^{(h)}}{\lambda^{(h)} \left(W_L^2 Z_1^{(h)} + W_1^2 Z_3^{(h)} \right)} e^{j30°} \dot{I}_{\alpha1}^{(h)} - \frac{\sqrt{3} W_2 W_L Z_1^{(h)} \left(W_L^2 Z_1^{(h)} + W_1^2 Z_3^{(h)} + 3W_1^2 Z_f^{(h)} \right)}{\lambda^{(h)} \left(W_L^2 Z_1^{(h)} + W_1^2 Z_3^{(h)} \right)} \dot{I}_{\alpha2}^{(h)} \\[3mm]
\dot{I}_{fa}^{(h)} = \dot{I}_{a3}^{(h)} + \dot{I}_{a4}^{(h)} = -\frac{\sqrt{3} W_2 W_L Z_1^{(h)} e^{j30°}}{\lambda^{(h)}} \left(\dot{I}_{\alpha1}^{(h)} + e^{-j30°} \dot{I}_{\alpha2}^{(h)} \right)
\end{cases}
\tag{18}
$$

Since inductive filtering is usually realized by using zero impedance, there is

$$Z_3^{(h)} = hZ_3 \approx 0 \tag{19}$$

Then, Equation (17) can be rewritten as:

$$\dot{I}_{A1}^{(h)} = \dot{I}_{A2}^{(h)} = \frac{3W_1 W_2 Z_f^{(h)}}{W_L^2 Z_1^{(h)} + 6W_1^2 Z_f^{(h)}} \left(\dot{I}_{\alpha1}^{(h)} + e^{-j30°} \dot{I}_{\alpha2}^{(h)} \right) \tag{20}$$

In addition, Equation (18) can be rewritten as:

$$
\begin{cases}
\dot{I}_{a3}^{(h)} = -\frac{\sqrt{3} W_2 \left(W_L^2 Z_1^{(h)} + 3W_1^2 Z_f^{(h)} \right) e^{j30°}}{W_L \left(W_L^2 Z_1^{(h)} + 6W_1^2 Z_f^{(h)} \right)} \dot{I}_{\alpha1}^{(h)} + \frac{3\sqrt{3} W_1^2 W_2 Z_f^{(h)} e^{j30°}}{W_L \left(W_L^2 Z_1^{(h)} + 6W_1^2 Z_f^{(h)} \right)} e^{-j30°} \dot{I}_{\alpha2}^{(h)} \\[3mm]
\dot{I}_{a4}^{(h)} = \frac{3\sqrt{3} W_1^2 W_2 Z_f^{(h)} e^{j30°}}{W_L \left(W_L^2 Z_1^{(h)} + 6W_1^2 Z_f^{(h)} \right)} \dot{I}_{\alpha1}^{(h)} - \frac{\sqrt{3} W_2 \left(W_L^2 Z_1^{(h)} + 3W_1^2 Z_f^{(h)} \right) e^{j30°}}{W_L \left(W_L^2 Z_1^{(h)} + 6W_1^2 Z_f^{(h)} \right)} e^{-j30°} \dot{I}_{\alpha2}^{(h)} \\[3mm]
\dot{I}_{fa}^{(h)} = \dot{I}_{a3}^{(h)} + \dot{I}_{a4}^{(h)} = -\frac{\sqrt{3} W_2 W_L Z_1^{(h)} e^{j30°}}{W_L^2 Z_1^{(h)} + 6W_1^2 Z_f^{(h)}} \left(\dot{I}_{\alpha1}^{(h)} + e^{-j30°} \dot{I}_{\alpha2}^{(h)} \right)
\end{cases}
\tag{21}
$$

Assume that the DC output current of the 12 pulse converter system based on the integrated multi-winding inductive filter converter transformer shown in Figure 1 is I_d. Taking the midpoint of the positive and negative half wave of the line current from the

star-connected winding at valve-side of the upper bridge as the zero point of time, then the basic expression of the line current of the star-connected winding at the valve-side of the upper bridge is presented in Equation (22) according to the harmonic characteristics of the three-phase full bridge rectifier circuit [16]:

$$
\begin{aligned}
i_{\alpha1} &= \frac{2\sqrt{3}}{\pi} I_d \left[\sin\omega t - \frac{1}{5}\sin 5\omega t - \frac{1}{7}\sin 7\omega t + \frac{1}{11}\sin 11\omega t + \frac{1}{13}\sin 13\omega t \right. \\
&\quad \left. - \frac{1}{17}\sin 17\omega t - \frac{1}{19}\sin 19\omega t + \ldots \right] \\
&= \frac{2\sqrt{3}I_d}{\pi}\sin\omega t + \frac{2\sqrt{3}I_d}{\pi}\sum_{\substack{n=6k\pm1 \\ k=1,2,3,\ldots}} (-1)^k \frac{\sin n\omega t}{n} \\
&= \frac{2\sqrt{3}I_d}{\pi}\sin\omega t - \frac{2\sqrt{3}I_d}{\pi}\sum_{n=12k-5} \frac{\sin n\omega t}{n} \\
&\quad - \frac{2\sqrt{3}I_d}{\pi}\sum_{n=12k-7} \frac{\sin n\omega t}{n} + \frac{2\sqrt{3}I_d}{\pi}\sum_{n=12k\pm1} \frac{\sin n\omega t}{n}
\end{aligned}
\tag{22}
$$

The valve-side of the lower bridge adopts delta connection, so its line current is $30°$ ahead of the one from the star-connected windings of upper bridge. Then, the expression of the line current from delta-connected winding at the valve-side can be deduced according to Equation (22):

$$
\begin{aligned}
&i_{\alpha2} = \frac{2\sqrt{3}}{\pi} I_d \left[\sin\left(\omega t + \tfrac{\pi}{6}\right) - \tfrac{1}{5}\sin 5\left(\omega t + \tfrac{\pi}{6}\right) - \tfrac{1}{7}\sin 7\left(\omega t + \tfrac{\pi}{6}\right) + \tfrac{1}{11}\sin 11\left(\omega t + \tfrac{\pi}{6}\right) \right. \\
&\qquad \left. + \tfrac{1}{13}\sin 13\left(\omega t + \tfrac{\pi}{6}\right) - \tfrac{1}{17}\sin 17\left(\omega t + \tfrac{\pi}{6}\right) - \tfrac{1}{19}\sin 19\left(\omega t + \tfrac{\pi}{6}\right) + \ldots \right] \\
&\quad = \frac{2\sqrt{3}I_d}{\pi}\sin\left(\omega t + \tfrac{\pi}{6}\right) + \frac{2\sqrt{3}I_d}{\pi}\sum_{\substack{n=6k\pm1 \\ k=1,2,3,\ldots}} (-1)^k \frac{\sin n\left(\omega t + \tfrac{\pi}{6}\right)}{n} \\
&\quad = \frac{2\sqrt{3}I_d}{\pi}\sin\left(\omega t + \tfrac{\pi}{6}\right) - \frac{2\sqrt{3}I_d}{\pi}\sum_{n=12k-5} \frac{\sin n\left(\omega t + \tfrac{\pi}{6}\right)}{n} - \frac{2\sqrt{3}I_d}{\pi}\sum_{n=12k-7} \frac{\sin n\left(\omega t + \tfrac{\pi}{6}\right)}{n} \\
&\qquad + \frac{2\sqrt{3}I_d}{\pi}\sum_{n=12k\pm1} \frac{\sin n\left(\omega t + \tfrac{\pi}{6}\right)}{n}
\end{aligned}
\tag{23}
$$

In the above equation, since the fundamental wave and the $6k + 1$-th harmonic are positive sequence components, and the $6k - 1$-th harmonic is a negative sequence component, the following equation can be obtained:

$$
\begin{aligned}
e^{-j30°} i_{\alpha2} &= \frac{2\sqrt{3}}{\pi} I_d \left\{ \sin\left[\left(\omega t + \tfrac{\pi}{6}\right) - \tfrac{\pi}{6}\right] - \tfrac{1}{5}\sin\left[5\left(\omega t + \tfrac{\pi}{6}\right) + \tfrac{\pi}{6}\right] - \tfrac{1}{7}\sin\left[7\left(\omega t + \tfrac{\pi}{6}\right) - \tfrac{\pi}{6}\right] \right. \\
&\qquad + \tfrac{1}{11}\sin\left[11\left(\omega t + \tfrac{\pi}{6}\right) + \tfrac{\pi}{6}\right] + \tfrac{1}{13}\sin\left[13\left(\omega t + \tfrac{\pi}{6}\right) - \tfrac{\pi}{6}\right] \\
&\qquad \left. - \tfrac{1}{17}\sin\left[17\left(\omega t + \tfrac{\pi}{6}\right) + \tfrac{\pi}{6}\right] - \tfrac{1}{19}\sin\left[19\left(\omega t + \tfrac{\pi}{6}\right) - \tfrac{\pi}{6}\right] + \ldots \right\} \\
&= \frac{2\sqrt{3}}{\pi} I_d \left[\sin\omega t + \tfrac{1}{5}\sin 5\omega t + \tfrac{1}{7}\sin 7\omega t + \tfrac{1}{11}\sin 11\omega t + \tfrac{1}{13}\sin 13\omega t \right. \\
&\qquad \left. + \tfrac{1}{17}\sin 17\omega t + \tfrac{1}{19}\sin 19\omega t + \ldots \right] \\
&= \frac{2\sqrt{3}I_d}{\pi}\sin\omega t + \frac{2\sqrt{3}I_d}{\pi}\sum_{n=12k-5} \frac{\sin n\omega t}{n} + \frac{2\sqrt{3}I_d}{\pi}\sum_{n=12k-7} \frac{\sin n\omega t}{n} \\
&\qquad + \frac{2\sqrt{3}I_d}{\pi}\sum_{n=12k\pm1} \frac{\sin n\omega t}{n}
\end{aligned}
\tag{23}
$$

By comparing and analyzing Equations (22) and (23), the following relationship can be acquired:

1. For the harmonic current on the order of $n = 12k \pm 1 (k = 1, 2, 3, \ldots)$, there is

$$
\dot{I}_{\alpha1}^{(n)} = e^{-j30°} \dot{I}_{\alpha2}^{(n)}
\tag{24}
$$

2.   For the harmonic current on the order of $n = 12k - 5, 12k - 7(k = 1, 2, 3, \ldots)$, there is

$$\dot{I}_{\alpha 1}^{(n)} = -e^{-j30°} \dot{I}_{\alpha 2}^{(n)} \tag{25}$$

Combining Equations (20), (24), and (25), the expression of a harmonic current from grid-side winding of upper and lower bridges is:

$$\dot{I}_{A1}^{(n)} = \dot{I}_{A2}^{(n)} = \begin{cases} 0, & n = 12k - 5, 12k - 7(k = 1, 2, 3, \ldots) \\ \dfrac{6W_1 W_2 Z_f^{(n)}}{W_L^2 Z_1^{(n)} + 6W_1^2 Z_f^{(n)}} \dot{I}_{\alpha 1}^{(n)}, & n = 12k \pm 1(k = 1, 2, 3, \ldots) \end{cases} \tag{26}$$

It can be seen from the above equation that, even if the filter device corresponding to $12k - 5, 12k - 7(k = 1, 2, 3, \ldots)$-th harmonic is not installed, harmonics of these orders as the 5th, 7th, 17th, and 19th harmonics do not exist at the grid-side winding, due to the parallel topology of two delta filters. If the 11th and 13th tuned filter devices are connected to the filter-side winding, then there is $Z_f^n \approx 0, n = 11, 13$. Combined with Equation (26), it can be obtained that the winding current at the grid-side also does not contain the 11th and 13th harmonics.

5. Transfer Path of Harmonic in Integrated Multi-Winding Inductive Filter Converter Transformer and Its Filter System

Next, the transfer path of each harmonic current will be analyzed and discussed. The transfer characteristics of a harmonic from an integrated multi-winding inductive filter converter transformer and its filter system are explored, and its unique advantages in harmonic suppression are analyzed.

5.1. Transfer Path Analysis of $12k - 5, 12k - 7(K = 1, 2, 3, \ldots)$-Th Harmonic Current
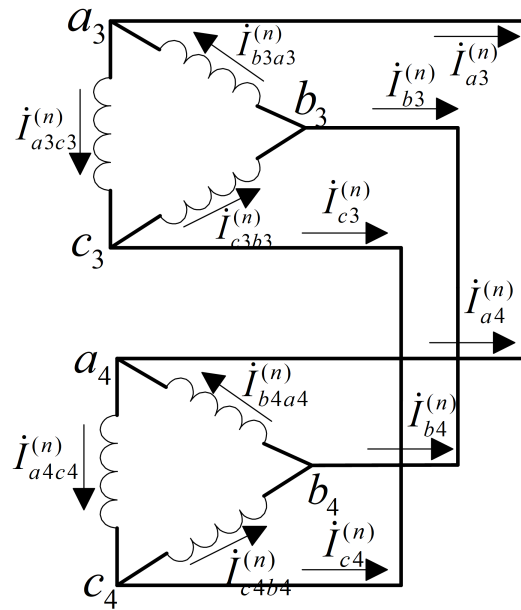
For the $12k - 5, 12k - 7(k = 1, 2, 3, \ldots)$-th harmonic current, the following equations can be obtained from Equations (21) and (25):

$$\begin{cases} \dot{I}_{a3}^{(n)} = -\dfrac{\sqrt{3}W_2\left(W_L^2 Z_1^{(n)} + 3W_1^2 Z_f^{(n)}\right)e^{j30°}}{W_L\left(W_L^2 Z_1^{(n)} + 6W_1^2 Z_f^{(n)}\right)} \dot{I}_{\alpha 1}^{(n)} + \dfrac{3\sqrt{3}W_1^2 W_2 Z_f^{(n)} e^{j30°}}{W_L\left(W_L^2 Z_1^{(n)} + 6W_1^2 Z_f^{(n)}\right)} e^{-j30°} \dot{I}_{\alpha 2}^{(n)} \\ \dot{I}_{a4}^{(n)} = -\dot{I}_{a3}^{(n)} = \dfrac{\sqrt{3}W_2\left(W_L^2 Z_1^{(n)} + 3W_1^2 Z_f^{(n)}\right)e^{j30°}}{W_L\left(W_L^2 Z_1^{(n)} + 6W_1^2 Z_f^{(n)}\right)} \dot{I}_{\alpha 1}^{(n)} - \dfrac{3\sqrt{3}W_1^2 W_2 Z_f^{(n)} e^{j30°}}{W_L\left(W_L^2 Z_1^{(n)} + 6W_1^2 Z_f^{(n)}\right)} e^{-j30°} \dot{I}_{\alpha 2}^{(n)} \\ \dot{I}_{fa}^{(n)} = \dot{I}_{a3}^{(n)} + \dot{I}_{a4}^{(n)} = 0 \end{cases} \tag{27}$$

Considering $Z_f^{(n)} \gg Z_1^{(n)}$, the above equations can be changed to:

$$\begin{cases} \dot{I}_{a3}^{(n)} = -\dfrac{\sqrt{3}W_2}{W_L} e^{j30°} \dot{I}_{\alpha 1}^{(n)} \\ \dot{I}_{a4}^{(n)} = -\dfrac{\sqrt{3}W_2}{W_L} \dot{I}_{\alpha 2}^{(n)} \\ \dot{I}_{a3}^{(n)} = -\dot{I}_{a4}^{(n)} \end{cases} \tag{28}$$

According to Equation (28), when the filter-side windings of the integrated multi-winding inductive filter converter transformer use zero impedance, since the two delta filter windings of the upper and lower bridge converter transformers are connected in parallel, and all the $12k - 5, 12k - 7(k = 1, 2, 3, \ldots)$-th harmonic currents generated by the bridge converter valves form a closed loop in the paralleled filter windings. The transfer path of $12k - 5, 12k - 7(k = 1, 2, 3, \ldots)$-th harmonic current is shown in the figure below Figure 2:

Figure 2. Transfer path of the $12k-5, 12k-7(k=1,2,3,\ldots)$-th harmonic current.

Next, the mechanism of $12k-5, 12k-7(k=1,2,3,\ldots)$-th harmonic suppression is revealed from the perspective of magnetic potential balance. From Figure 2, the magnetic potential equation of $12k-5, 12k-7(k=1,2,3,\ldots)$-th harmonic in the upper and lower bridge valve-side windings and filter-side windings of the integrated multi-winding inductive filter converter transformer can be obtained as below:

$$\frac{W_2}{W_1}\dot{I}_{a1}^{(n)}+\frac{W_L}{W_1}\dot{I}_{a3c3}^{(n)}+\frac{W_3}{W_1}\dot{I}_{a2c2}^{(n)}+\frac{W_L}{W_1}\dot{I}_{a4c4}^{(n)}=-\frac{W_2}{W_1}\dot{I}_{\alpha1}^{(n)}-\frac{W_Le^{-j30°}}{\sqrt{3}W_1}\dot{I}_{a3}^{(n)}-\frac{\sqrt{3}W_2e^{-j30°}}{\sqrt{3}W_1}\dot{I}_{\alpha2}^{(n)}-\frac{W_Le^{-j30°}}{\sqrt{3}W_1}\dot{I}_{a4}^{(n)} \tag{29}$$

Substituting Equation (28) into Equation (29), there is

$$\frac{W_2}{W_1}\dot{I}_{a1}^{(n)}+\frac{W_L}{W_1}\dot{I}_{a3c3}^{(n)}+\frac{W_3}{W_1}\dot{I}_{a2c2}^{(n)}+\frac{W_L}{W_1}\dot{I}_{a4c4}^{(n)}=0 \tag{30}$$

Combining the transfer path of $12k-5, 12k-7(k=1,2,3,\ldots)$-th harmonic current in Figure 2 with Equation (30), it can be seen that a superconductivity closed-loop for the $12k-5, 12k-7(k=1,2,3,\ldots)$-th harmonic current is formed by the two paralleled-connected delta filters that adopted a unique zero impedance design. That is, no matter how the harmonic flux of the closed loop of the superconductor changes, the harmonic flux generated by the harmonic current induced by the loop will always resist this change. Therefore, the harmonic magnetomotive force balance is achieved between the filter-side winding and the valve-side winding at the $12k-5, 12k-7(k=1,2,3,\ldots)$-th harmonic frequencies, that is, Equation (30) is established, so as to eliminate the $12k-5, 12k-7(k=1,2,3,\ldots)$-th harmonic magnetic flux in the core. On this basis, the grid-side winding will not induce the harmonic current of specific harmonic frequency, which means the proposed inductive filter converter transformer shields the harmonic current from its valve-side winding to realize the isolation from the grid-side winding and AC power grid. This harmonic control method is similar to the effect of phase-shifting and confluence elimination of the $12k-5, 12k-7(k=1,2,3,\ldots)$-th harmonic at the grid-side in the traditional 12 pulse converter circuit, but it is not the same. Since the confluence here is in the filter winding on the valve-side, the harmonic will not be transferred to the grid-side side. Thus, the harmonic suppression near the valve-side is realized, and the negative impact of the $12k-5, 12k-7(k=1,2,3,\ldots)$-th harmonic on the transformer body in the transferring process is reduced, such as harmonic loss, vibration, and noise.

From the above analysis, it can be seen that the $12k - 5, 12k - 7 (k = 1, 2, 3, \ldots)$-th harmonics can be effectively suppressed with no corresponding filtering branches if the two delta windings designed with zero impedance are parallel-connected. That is, the desired harmonic suppression can be realized without installing 5th and 7th harmonic filters, which reduces the cost of harmonic treatment.

5.2. Transfer Path Analysis of the 11th and 13th Harmonic Current

To control the 11th and 13th harmonics, the corresponding tuned filter devices are connected at the parallel tap of the delta filter winding. Then, the following equation is established:

$$Z_f^{(n)} \approx 0, \quad n = 11, 13 \tag{31}$$

Substituting Equation (31) into Equation (26), there is

$$\dot{I}_{A1}^{(n)} = \dot{I}_{A2}^{(n)} = \frac{6W_1 W_2 Z_f^{(n)}}{W_L^2 Z_1^{(n)} + 6W_1^2 Z_f^{(n)}} \dot{I}_{\alpha 1}^{(n)} = 0, \quad n = 1113 \tag{32}$$

It can be seen from the above equation that, after connecting the 11th and 13th tuned filter devices at the parallel taps of the two filter windings of the proposed inductive filter converter transformer, the 11th and 13th harmonic are not included in the winding current at the grid-side, that is, the 11th and 13th harmonic currents are suppressed. The following contents will focus on analyzing the transfer path of 11th and 13th harmonic currents, and deeply prompting its harmonic suppression mechanism. The following equations can be obtained from Equations (21), (24), and (31)

$$\begin{cases} \dot{I}_{a3}^{(n)} = \frac{-\sqrt{3}W_2}{W_L} e^{j30°} \dot{I}_{\alpha 1}^{(n)} \\ \dot{I}_{a4}^{(n)} = \frac{-\sqrt{3}W_2}{W_L} \dot{I}_{\alpha 2}^{(n)} \\ \dot{I}_{fa}^{(n)} = \dot{I}_{a3}^{(n)} + \dot{I}_{a4}^{(n)} = \frac{-\sqrt{3}W_2}{W_L} \left(e^{j30°} \dot{I}_{\alpha 1}^{(n)} + \dot{I}_{\alpha 2}^{(n)} \right) \end{cases} \tag{33}$$

According to Equation (33) and Figure 1, the transfer path of harmonic currents with order of is shown in the Figure 3:
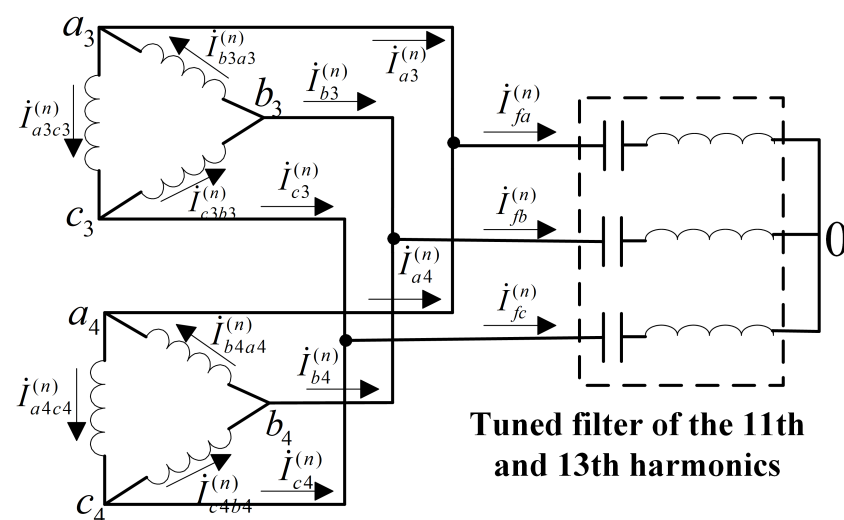
Figure 3. Transfer path of the 11th and 13th harmonic current.

As can be seen from Equation (33) and Figure 3, when 11th and 13th tuned filter devices are connected at the parallel taps, all the 11th and 13th harmonic currents generated by the upper and lower bridge converter valves are drained to the filter circuit composed

of filter-side windings and tuned filters. On this basis, the 11th and 13th harmonic currents are not contained in the grid-side winding. Substituting Equations (24) and (33) into Equation (29), there is

$$\frac{W_2}{W_1}\dot{I}_{a1}^{(n)} + \frac{W_L}{W_1}\dot{I}_{a3c3}^{(n)} + \frac{W_3}{W_1}\dot{I}_{a2c2}^{(n)} + \frac{W_L}{W_1}\dot{I}_{a4c4}^{(n)} = 0 \tag{34}$$

Combining the transfer path of 11th and 13th harmonic currents in Figure 3 with Equation (34), it can be seen that a superconductivity closed-loop for the 11th and 13th harmonic current is formed by the two paralleled-connected delta filters that use zero impedance. That is, no matter how the harmonic flux of the closed loop of the superconductor changes, the harmonic flux generated by the harmonic current induced by the loop will always resist this change. Therefore, the harmonic magnetomotive force balance is achieved between the filter-side and the valve-side at the 11th and 13th harmonic frequencies, that is, Equation (34) is established, so as to eliminate harmonic magnetic flux of the same order. On this basis, the grid-side winding will not induce the harmonic current of specific harmonic frequency, so the 11th and 13th harmonic currents can be shielded from the valve-side winding of converter transformer. Moreover, it can realize the isolation from the primary grid, and reduce the negative impact of 11th and 13th harmonics on the transformer.

5.3. Transfer Path Analysis of the 3rd Harmonic Current

The 3rd harmonic has the highest content in the excitation current of the converter transformer. The 3rd harmonic current is the zero sequence current, and the three-phase zero sequence current has the same size and phase, and its flow path is related to the connection group of transformer winding, including three cases. First, the three-phase windings are often star-connected, when there is no neutral wire, the zero sequence current cannot pass through, but it can flow in the windings when there is no neutral wire. When the the three-phase windings are delta-connected, the windings form a closed loop for the 3rd harmonic current. In this case, the 3rd harmonic current flows in the delta-winding, and there is no zero sequence current in the line current.

In the proposed inductive filter converter transformer, the primary winding adopts a star connection with a neutral wire, the upper bridge windings on the secondary side are star-connected with a neutral wire while the lower bridge winding is with a delta connection, and the two bridges are delta-connected. Therefore, the 3rd harmonic current will flow in each winding of the primary side and the secondary side, and will be distributed inversely according to the impedance of the flow path.

The two filters that are paralleled-connected in the converter transformer adopt a unique zero impedance design, and the windings in filters are connected by a delta structure. Therefore, a superconductivity closed-loop for the 3rd harmonic current is formed. The main advantage of this structure is that it can drain all of the 3rd harmonic current in the excitation current to the filter winding to prevent it from transforming to the primary side. On the other hand, it can realize the complete isolation and shielding of the 3rd harmonic current between grid-side and valve-side. In other words, when the two load windings on the valve-side contain the 3rd harmonic current, the 3rd harmonic current will only be induced to the two zero impedance filter windings. The transfer path of 3rd harmonic current in the inductive filtering transformer with two paralleled-connected delta filter windings is shown in Figure 4.

Taking the traditional 12 pulse converter transformer as a comparison, its the winding on the valve-side of the lower bridge is also delta-connected, but the 3rd harmonic current will be distributed inversely according to the impedance of the flow path since impedance is not zero. Therefore, the traditional one can only partially isolate and shield the 3rd harmonic current, that is, part of the 3rd harmonic current in the excitation current will be transmitted to the delta connection winding on the valve-side and part to the star connection winding with neutral wire on the grid-side.
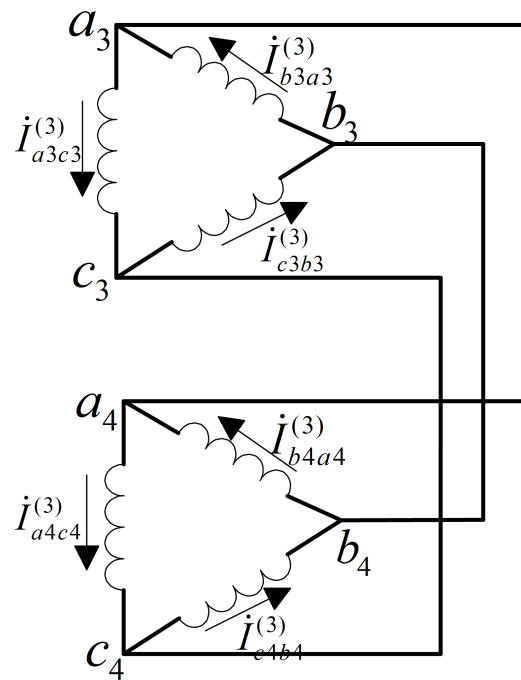
Figure 4. Transfer path of the 3rd harmonic current.

6. Analysis of Simulation and Experiment Results

6.1. Simulation Model

To verify the correctness of the above theoretical analysis, the simulation model of the integrated multi-winding inductive filter converter transformer and its filter system corresponding to Figure 1 is established by MATLAB/SIMULINK, as shown in Figure 5.
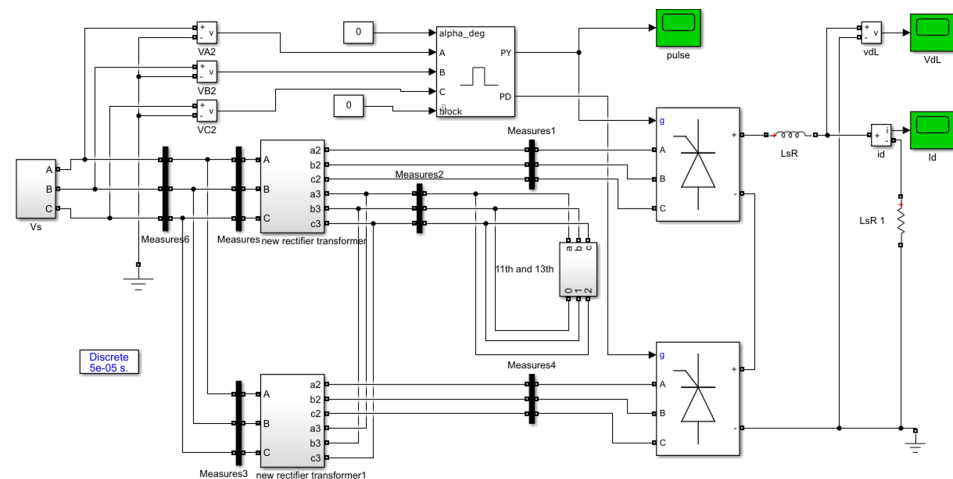

Figure 5. Simulation model of an integrated multi-winding inductive filter converter transformer and its filter system.

The basic parameters of simulation model are as follows:

(1) The power supply at the AC network is a three-phase symmetrical sinusoidal power supply with a voltage of 220 V and a frequency of 50 Hz.

(2) The integrated multi-winding inductive filter converter transformer is composed of three converter transformers with the same structure of a single-phase dual-column yoke-type and the same capacity of 20 KVA according to the wiring scheme in Figure 1. The specific parameters are shown in Table 1.

(3) DC rated voltage $Ud = 1000$ V, rated current $Id = 100$ A, rated power $Pd = 100$ kW, a rectifier adopts three-phase fully controlled bridge, and smoothing reactor $Ld = 9$ mh.

(4) To suppress the 11th and 13th harmonics, the parameters of a tuned filter adopted by the inductive filter converter transformer with parallel topology of double delta filter windings, and its filter system are shown in Table 2.

Table 1. Rated parameters of the novel single-phase inductive filter converter transformer.

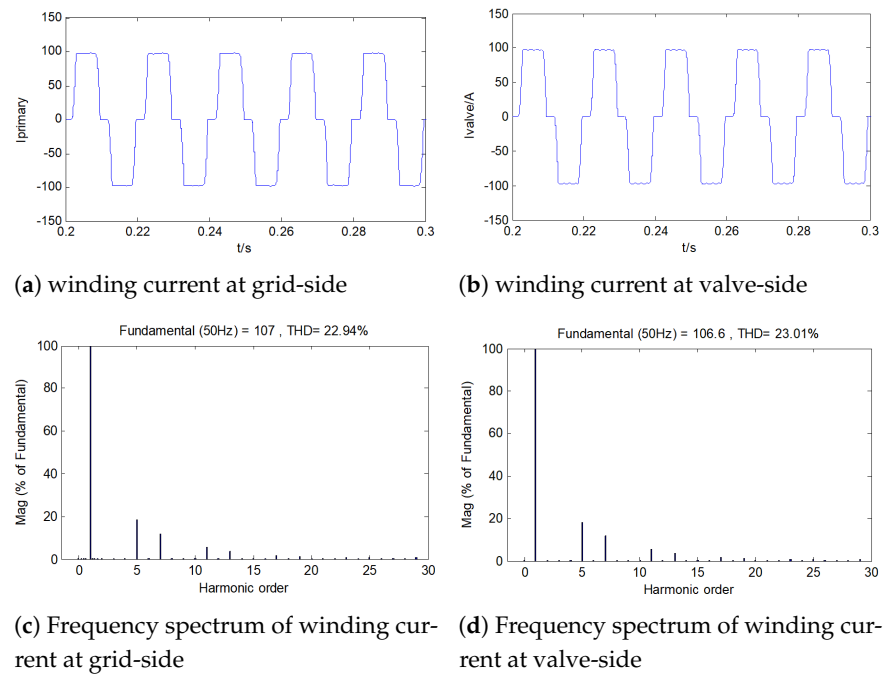| Rated Parameters	
Capacity/kVA	20
Voltage (grid-side/filter-side/valve-side with star connection)/V	219.39/380/219.38
Voltage (grid-side/filter-side/valve-side with delta connection)/V	219.39/380/380
Current (grid-side/filter-side/valve-side with star connection)/A	91.16/21.05/91.16
Current (grid-side/filter-side/valve-side with delta connection)/A	91.16/21.05/52.63
Frequency/Hz	50
Number of phases	Single phase

Table 2. Basic parameters of the inductive filter device with a double tuning structure.

| Filter Type	Series Section		Parallel Section	
	Capacitor/µF	Reactor/mH	Capacitor/µF	Reactor/mH
DT11/13	416.3	0.17006	14895	0.004757

6.2. Analysis of Simulation Results

According to the simulation model established in Figure 5, a comparative simulation analysis on transfer characteristics of harmonic for the proposed filter converter transformer is made, and it is carried out under the following three working conditions. Working condition 1: two delta filter windings are not parallel-connected and the filters are not put into use. Working condition 2: two delta filter windings are parallel-connected, and the filters are not put into use. Working condition 3: two delta filter windings are parallel-connected, and the 11th and 13th filters are put into use.
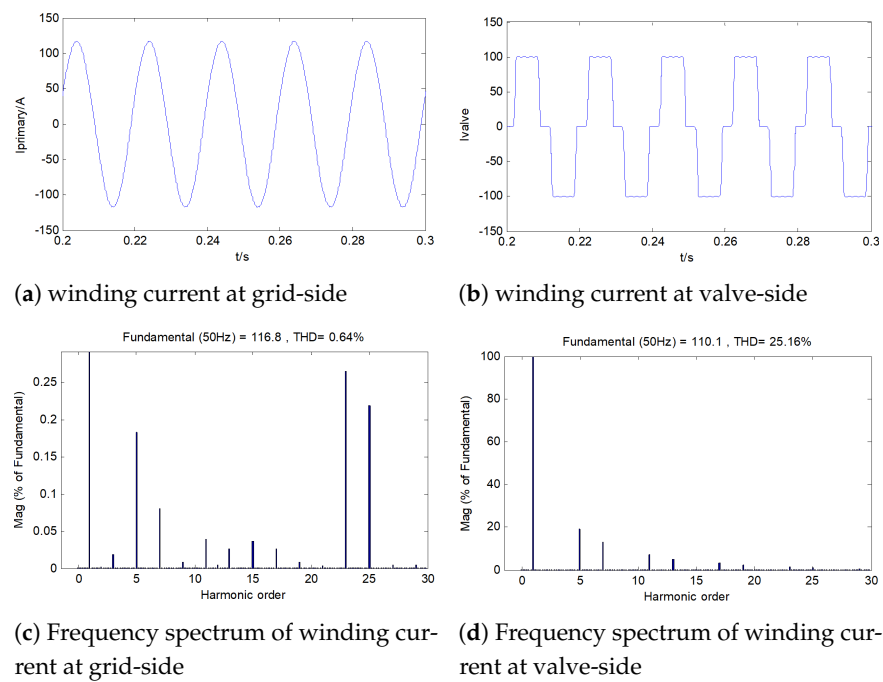
Figures 6–8 show a waveform and frequency spectrum of winding current from valve-side and grid-side on the columns of converter transformer under three working conditions. As can be seen from Figure 6, under working condition 1, the winding current waveforms at the grid-side and valve-side of converter transformer are similar and seriously distorted, and the total harmonic distortion rate is as high as 23.01%. This shows that, under condition 1, all harmonic currents generated by the converter valve are freely transferred through the transformer. However, in Figure 7, under condition 2, when two delta filter windings are parallel-connected and the filters are not put into use, the winding current at the valve-side is still seriously distorted, but the winding current waveform at the grid-side has been greatly improved, which is approximately the sine wave. Through FFT analysis, it can be seen that the content of 5th, 7th, 17th, and 19th harmonic currents, that is, the content of the $n = 12k - 5, 12k - 7$-th harmonic is low, the content of 11th and 13th harmonics is still high, and the total harmonic distortion rate is 8.05%. This shows that the parallel connection of two delta filter windings can suppress the $n = 12k - 5, 12k - 7$-th harmonic. This conclusion is consistent with the previous theoretical analysis about the transfer path of harmonic, and the proposed topology will save the cost of 5th and 7th harmonic filters. In Figure 8, under working condition 3, the waveform at the valve-side is still seriously distorted due to the commutation characteristics of the converter, but the winding current waveform at the grid-side is sinusoidal, and the total harmonic distortion rate is 0.64%. The FFT analysis shows that the 5th, 7th, 11th, 13th, 17th, and 19th harmonics have been effectively suppressed, so the harmonic content is very low. This means that the parallel connection of two delta filter windings can suppress the 5th, 7th, 17th, and 19th harmonics, and the use of the 11th and 13th filter can better suppress the corresponding harmonic, it is also consistent with the previous theoretical analysis.

(**a**) winding current at grid-side

(**b**) winding current at valve-side

(**c**) Frequency spectrum of winding current at grid-side

(**d**) Frequency spectrum of winding current at valve-side

Figure 6. Waveform and frequency spectrum of winding current from the valve-side and grid-side on the left column of the converter transformer under working condition 1.
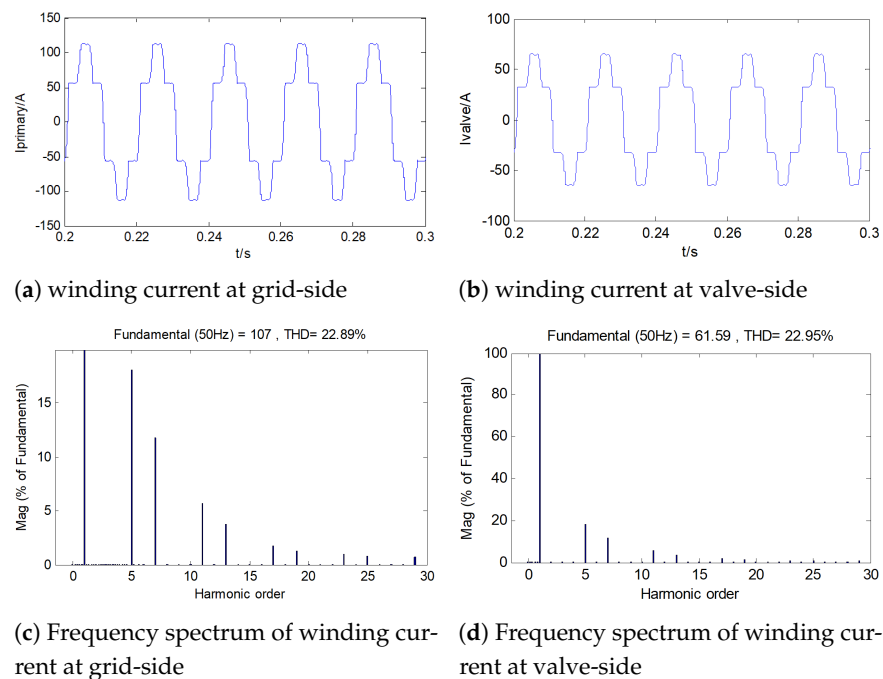

(**a**) winding current at grid-side

(**b**) winding current at valve-side

(**c**) Frequency spectrum of winding current at grid-side

(**d**) Frequency spectrum of winding current at valve-side
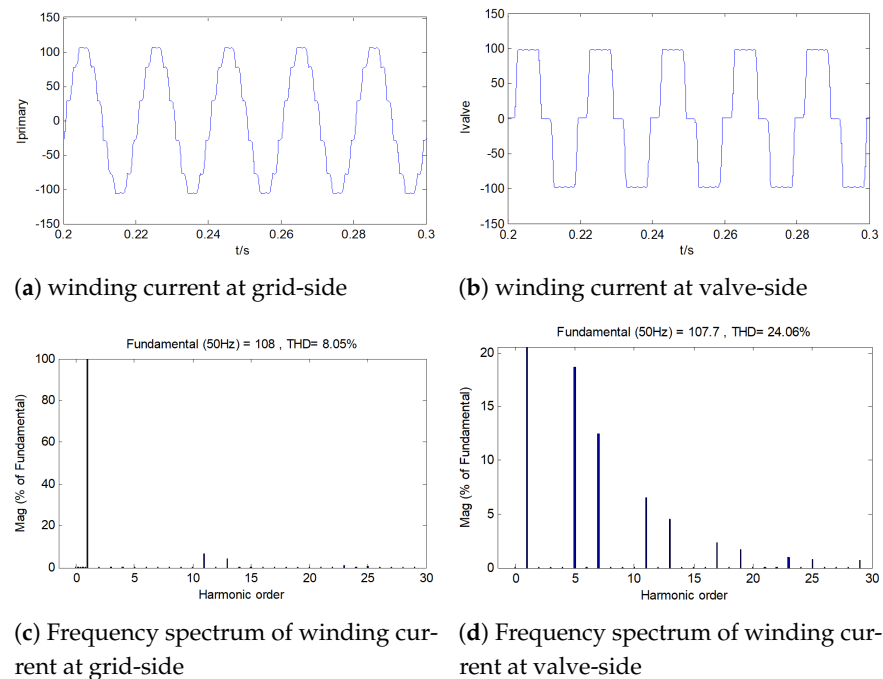
Figure 7. Waveformand frequency spectrum of winding current from the valve-side and grid-side on the left column of the converter transformer under working condition 2.
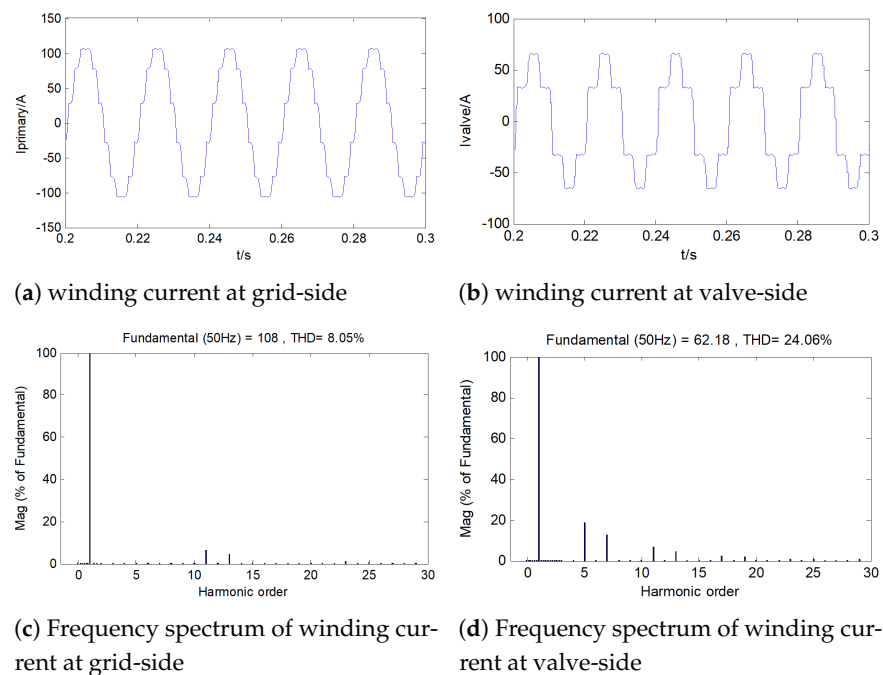
(**a**) winding current at grid-side

(**b**) winding current at valve-side

(**c**) Frequency spectrum of winding current at grid-side

(**d**) Frequency spectrum of winding current at valve-side

Figure 8. Waveformand frequency spectrum of the winding current from the valve-side and grid-side on the left column of the converter transformer under working condition 3.
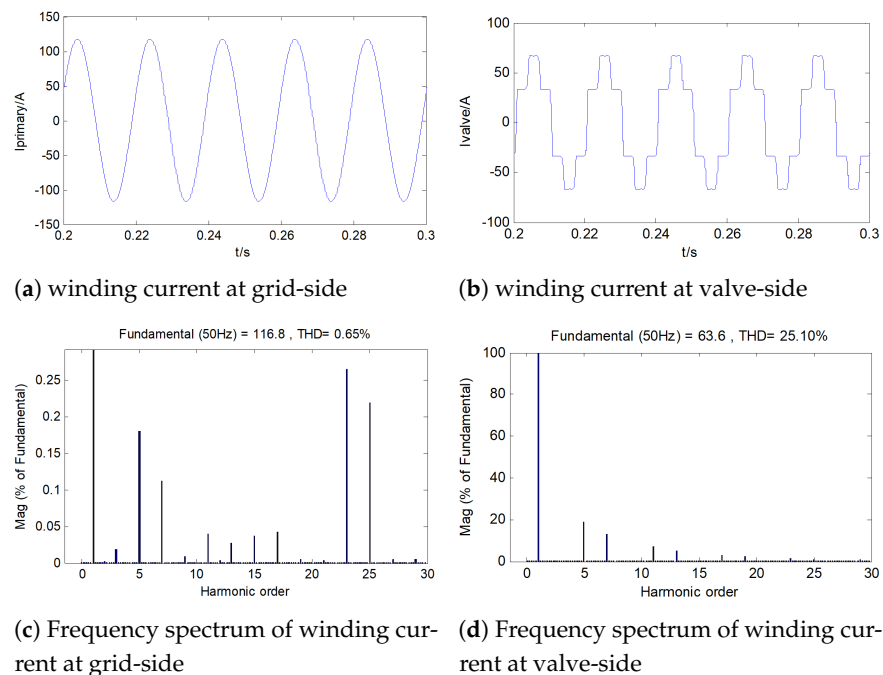
Figures 9–11 show waveform and frequency spectrum of winding current from valve-side and grid-side on the right column of the converter transformer under three working conditions, respectively.

(**a**) winding current at grid-side

(**b**) winding current at valve-side

(**c**) Frequency spectrum of winding current at grid-side

(**d**) Frequency spectrum of winding current at valve-side

Figure 9. Waveform and frequency spectrum of the winding current from the valve-side and grid-side on the right column of the converter transformer under working condition 1.

(**a**) winding current at grid-side

(**b**) winding current at valve-side

(**c**) Frequency spectrum of winding current at grid-side

(**d**) Frequency spectrum of winding current at valve-side

Figure 10. Waveform and frequency spectrum of winding current from the valve-side and grid-side on the right column of the converter transformer under working condition 2.

(**a**) winding current at grid-side

(**b**) winding current at valve-side

(**c**) Frequency spectrum of winding current at grid-side

(**d**) Frequency spectrum of winding current at valve-side

Figure 11. Waveform and frequency spectrum of the winding current from the valve-side and grid-side on the right column of the converter transformer under working condition 3.

From the simulation results, it can be seen that the current waveforms of the grid side and valve side windings of the right column converter transformer are different when using YDD connection and YYD connection. However, after FFT analysis, it is found that the main characteristic subharmonic contents of the left and right columns with different connection modes are basically the same.

Table 3 shows the simulation calculation results of fundamental current and 3rd, 5th, 7th, 11th, 13th, 17th, and 19th harmonic currents of grid-side and valve-side windings of
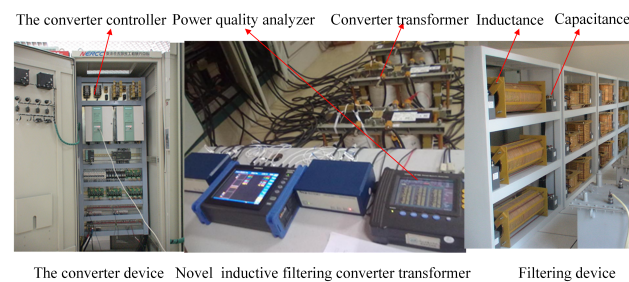
the inductive filter converter transformer with parallel topology of two delta filter windings under three working conditions.

Table 3. Simulation results of winding current at the grid-side and winding current at the valve-side of the integrated multi-winding inductive filter converter transformer

| Bridge	Working Condition	Winding	Current Amplitude/A								THD/%
			1	3	5	7	11	13	17	19	
Upper bridge YYD	working condition 1	grid-side	106.96	0.05	19.46	12.64	6.06	4.07	1.89	1.36	22.94
		valve-side	106.63	0.05	19.46	12.64	6.06	4.07	1.89	1.36	23.01
	working condition 2	grid-side	108.01	0.02	0.21	0.13	6.99	4.84	0.03	0.01	8.05
		valve-side	107.7	0.03	20.11	13.4	6.99	4.85	2.54	1.83	24.06
	working condition 3	grid-side	116.8	0.02	0.21	0.09	0.05	0.03	0.03	0.01	0.64
		valve-side	110.1	0.03	21.0	14.28	8.02	5.72	3.44	2.62	25.16
Lower bridge YDD	working condition 1	grid-side	106.98	0.06	19.42	12.63	6.03	4.04	1.91	1.35	22.89
		valve-side	61.59	0.03	11.21	7.29	3.48	2.33	1.10	0.78	22.95
	working condition 2	grid-side	107.96	0.02	0.20	0.06	6.99	4.84	0.05	0.01	8.05
		valve-side	62.18	0.03	11.6	7.74	4.03	2.79	1.48	1.04	24.06
	working condition 3	grid-side	116.84	0.02	0.21	0.13	0.05	0.03	0.05	0.01	0.65
		valve-side	63.6	0.03	12.11	8.24	4.7	3.28	1.96	1.48	25.1

6.3. Analysis of Experiment Results

A prototype of integrated multi-winding inductive filter converter transformer is designed and manufactured to verify the correctness of the proposed theoretical analysis. The harmonic suppression characteristics are experimentally studied according to the original DC transmission platform in the laboratory. The instrument used for the test is power quality analyzer HIOKI3196. Figure 12 shows the wiring diagram of experiments.


Figure 12. Wiring diagram of experiment for the integrated multi-winding inductive filter converter transformer.
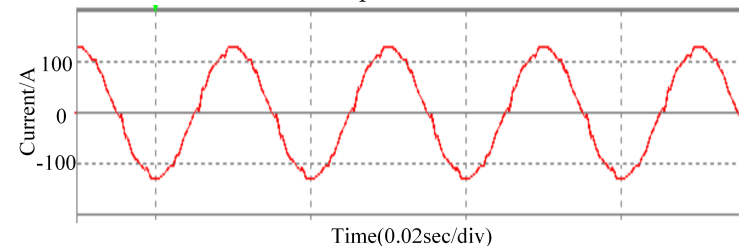
In Figure 13, the measured waveform of winding current at the grid-side of the inductive filter converter transformer under three working conditions are presented. Moreover, Table 4 and Figure 14 shows harmonic content in measured current at grid-side winding under three working conditions.
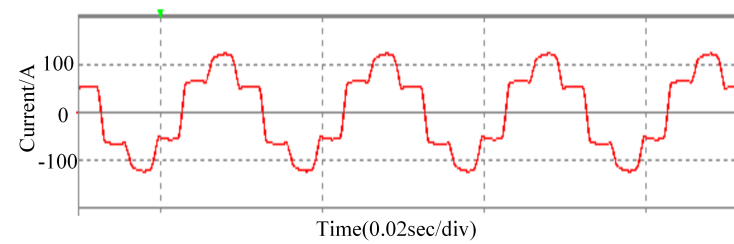
(**a**) working condition 1: two delta filter windings are not parallel-connected and the filters are not put into use
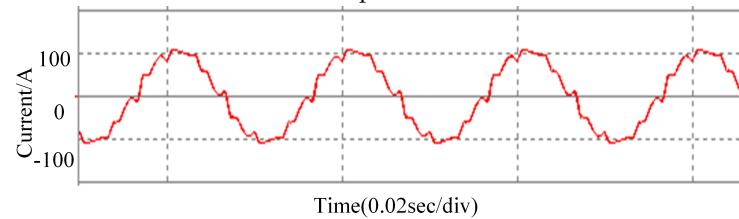

(**b**) working condition 2: two delta filter windings are parallel-connected and the filters are not put into use

(**c**) working condition 3: two delta filter windings are parallel-connected and the 11th and 13th filters are put into use

Figure 13. Measured waveform of winding current at the grid-side of the inductive filter converter transformer under three working conditions.
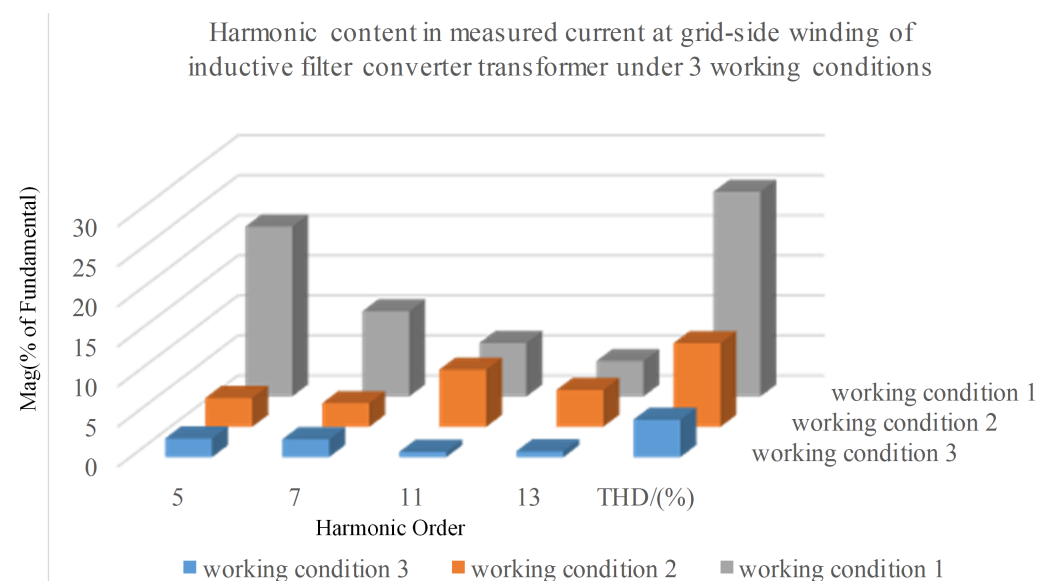
Figure 14. The histogram of harmonic content in measured current at the grid-side winding of the inductive filter converter transformer under three working conditions.

Table 4. Harmonic content in measured current at grid-side winding of the inductive filter converter transformer under three working conditions.

Working Condition	Harmonic Content in Winding Current at Grid-Side/(%)				THD/(%)
	5	7	11	13	
working condition 1	21.23	10.64	6.69	4.43	25.58
working condition 2	3.62	2.96	7.15	4.62	10.46
working condition 3	2.35	2.24	0.67	0.75	4.68

According to Table 2 and the comparative analysis of Figure 13a,b, when two delta filter windings are connected in parallel without filter, the $n = 12k - 5, 12k - 7$-th harmonic in the grid-side winding of converter transformer is suppressed, which significantly improves the waveform. The 5th and 7th harmonic contents are reduced from 21.23% and 10.64% to 3.26% and 2.96%, respectively, and the total harmonic distortion rate is reduced from 25.58% to 10.46%. As shown in Figure 13c, when two delta filter windings are connected in parallel and connected to 11th and 13th tuned harmonic filters, the winding current on the grid-side is approximately sine wave, and the total harmonic distortion rate is reduced to 4.68%, which is consistent with the previous theoretical analysis results.

7. Conclusions

For problems such as harmonic suppression and reactive power compensation that occupied an important position in the field of AC and DC power conversion, an integrated multi-winding inductive filter converter and its filter system used in HVDC conversion station were studied in this paper. The mathematical model of inductive filtering transformer with two paralleled-connected delta filter windings and its filter system were established. The current relationships between different windings were derived, and the harmonic current paths and reactive power compensation characteristics of this new system were demonstrated. In addition, the system simulation model was established and the physical platform of the system was built. The following conclusions could be drawn through the experiment.

(1) In the proposed system, the parallel connection of two delta filter windings with zero impedance could change the transfer path of harmonics, so that all the $12k - 5, 12k - 7 (k = 1, 2, 3, \ldots)$-th harmonic currents generated by the upper and lower bridge converter valves formed a closed loop in the two parallel filter windings. On this basis, it could prevent the $12k - 5, 12k - 7 (k = 1, 2, 3, \ldots)$-th harmonic from transferring to the grid-side winding, and the 5th and 7th harmonic filters could be eliminated while the corresponding harmonics could still be suppressed, which reduced the harmonic treatment cost. The experimental results show that the total harmonic distortion rate of the grid-winding current can be reduced to 10.46% when two delta filter windings are parallel-connected, and the 11th and 13th filters are not put into use.

(2) The 11th and 13th tuned filter branches that connected at the parallel taps of two delta filter windings could drain all the corresponding harmonic currents to the filter circuit. Therefore, the 11th and 13th harmonic currents were not contained in the grid-side and were shielded from the valve-side winding. It realized the isolation of harmonic current from grid-side winding and AC power grid, as well as the reduction of the negative impact of 11th and 13th harmonics on the transformer body in the transferring process, such as harmonic loss, vibration, and noise. The experimental results show that the total harmonic distortion rate of the grid-winding current can be reduced to 4.68% when two delta filter windings are parallel-connected and the 11th and 13th filters are only installed, so as the effect of active filtering is approximated realized by the passive filtering method.

(3) Due to the zero impedance and delta connection of windings in the two paralleled-connected filters, a superconductivity closed-loop for the 3rd harmonic current was formed. The advantages of this structure were specifically reflected in two aspects. First, it could drain all of the 3rd harmonic current in the excitation current to the filter winding to prevent it from transferring to the primary side. On the other hand, it could realize the complete isolation and shielding of the 3rd harmonic current between grid-side and valve-side. In other words, when the two load windings on the valve-side contained the 3rd harmonic current, the 3rd harmonic current would only be induced to the two zero impedance filter windings. For the traditional 12 pulse converter transformer, although the winding on the valve-side of the lower bridge was also delta-connected, the 3rd harmonic current would be distributed inversely according to the impedance of the transfer path since impedance was not zero. Therefore, it could only partially isolate and shield the 3rd harmonic current.

References

1. Ellis, R.G. Harmonic analysis of industrial power systems. *IEEE Trans. Ind. Appl.* **1996**, *32*, 417–421. [CrossRef]
2. Singh, G.K. Power system harmonics research: A survey. *Eur. Trans. Electr. Power* **2009**, *19*, 151–172. [CrossRef]
3. Sher, H.A.; Addoweesh, K.E.; Khan, Y. Harmonics generation, propagation and purging techniques in non-linear loads. In *An Update on Power Quality*; Intech Open: Rijeka, Croatia, 2013. [CrossRef]
4. Sun, J.; Li, M.; Zhang, Z.; Xu, T.; He, J.; Wang, H.; Li, G. Renewable energy transmission by HVDC across the continent: System challenges and opportunities. *CSEE J. Power Energy Syst.* **2017**, *3*, 353–364.
5. Das, S.R.; Ray, P.K.; Sahoo, A.K.; Ramasubbareddy, S.; Babu, T.S.; Kumar, N.M.; Elavarasan, R.M.; Mihet-Popa, L. A Comprehensive Survey on Different Control Strategies and Applications of Active Power Filters for Power Quality Improvement. *Energies* **2021**, *14*, 4589.
6. Wang, Y.B.; Lv, Y.; Tian, Z.G.; Xu, Zhen. Improvement of the Control Technique for the Harmonic Suppression and Reactive Compensation Device. *Electr. Meas. Instrum.* **2006**, *43*, 4. [CrossRef]
7. Li, Y.Q.; Chen, Z.Y.; Li, P.; Xie, H.L. Review on Harmonic Restraining Technology in Power System. *J. North China Electr. Power Univ.* **1995**, *28*, 19–22. [CrossRef]
8. Geng, D.Y.; Wang, F.X. Phase-shifting Reactor—A New Method for Converter Power Supply Systems Harmonic Suppression. *J. Liaoning Inst. Technol. Sci. Ed.* **2003**, *23*, 16–20. [CrossRef]
9. Dehghani, M.; Niknam, T.; Ghiasi, M.; Baghaee, H.R.; Blaabjerg, F.; Dragicević, T.; Rashidi, M. Adaptive backstepping control for master-slave AC microgrid in smart island. *Energy* **2022**, *246*, 123282. [CrossRef]
10. Dehghani, M.; Kavousi-Fard, A.; Niknam, T.; Avatefipour, O. A robust voltage and current controller of parallel inverters in smart island: A novel approach. *Energy* **2021**, *214*, 118879. [CrossRef]
11. Wang, F.X.; Geng, D.Y. Study on harmonic repression of converter-fed power system by using phase-shifting reactor. *Proc. CSEE* **2003**, *23*, 54–57.
12. Forrest, J.A.C.; Allard, B. Thermal problems caused by harmonic frequency leakage fluxes in three-phase, three-winding converter transformers. *IEEE Trans. Power Deliv.* **2004**, *19*, 208–213.
13. Wagner, V.E.; Balda, J.C.; Griffith, D.C.; Mceachern, A.; Barnes, T.M.; Hartmann, D.P.; Phileggi, D.J.; Emannuel, A.E.; Horton, W.F.; Reid, W.E.; et al. Effects of harmonics on equipment. *IEEE Trans. Power Deliv.* **1993**, *8*, 672–680. [CrossRef]
14. Pierce, L.W. Transformer design and application considerations for nonsinusoidal load currents. *IEEE Trans. Ind. Appl.* **1996**, *32*, 633–645. [CrossRef]

15. Kennedy, S.P.; Ivey, C.L. Application, design and rating of transformers containing harmonic currents. In Proceedings of the Annual Technical Conference on Pulp and Paper Industry, Seattle, WA, USA, 18–22 June 1990; pp. 19–31.

16. Li, Y.; Luo, L.; Liu, F. Application Foreground of Transformer Inductive Filtering Technology *Trans. China Electrotech. Soc.* **2009**, *24*, 86–92. [CrossRef]

17. Luo, L.; Li, Y.; Xu, J.; Li, J.; Hu, B.; Liu, F. A new converter transformer and a corresponding inductive filtering method for HVDC transmission system. *IEEE Trans. Power Deliv.* **2008**, *23*, 1426–1431. [CrossRef]

18. Li, Y.; Luo, L.; Rehtanz, C.; Nakamura, K.; Xu, J.; Liu, F. Study on characteristic parameters of a new converter transformer for HVDC systems. *IEEE Trans. Power Deliv.* **2009**, *24*, 2125–2131. [CrossRef]

19. Ngoc, T.T.; Luo, L.F.; Xu, J.Z.; Dong, S. Influence of inductive filters on short-circuit impedances of new converter transformer. *Trans. China Electrotech. Soc.* **2012**, *27*, 71–76.

20. Cui, G.; Luo, L.; Li, Y.; Liang, C.; Hu, S.; Xie, B.; Xu, J.; Zhang, Z.; Liu, Y.; Wang, T. YN/VD connected balance transformer-based hybrid power quality compensator for harmonic suppression and reactive power compensation of electrical railway power systems. *Int. J. Electr. Power Energy Syst.* **2019**, *113*, 481–491.

21. Liu, Q.; Li, Y.; Hu, S.; Luo, L. A Transformer Integrated Filtering System for Power Quality Improvement of Industrial DC Supply System. *IEEE Trans. Ind. Electron.* **2019**, *67*, 3329–3339. [CrossRef]

22. Liu, Q.; Li, Y.; Hu, S.; Luo, L.; Cao, Y. Study on Filtering Mechanism and Operating Characteristic of the Controllably Inductive Power Filtering System. *Diangong Jishu Xuebao/Trans. China Electrotech. Soc.* **2018**, *33*, 3274–3283.

23. Tian, Y.; Luo, L.F.; Li, Y.; Huang, Z.; Liu, Q.Y. Performance Analysis and Port Matrix Model of 220 kV Multi-winding Inductively Filtered Transformer. *Proc. CSEE* **2020**, *40*, 3042–3051. [CrossRef]

24. Huang, Z.; Luo, L.F.; Li, Y.; Shi, S.M.; Tian, Y. Research the Operating Characteristics of Four-winding Inductive Filtering Transformer Based on the Port Model. *Proc. CSEE* **2019**, *39*, 6706–6715. [CrossRef]

25. Li, J.Y.; Luo, L.F.; Xu, J.Z. A Harmonic Suppression Rectifier Transformer with Filters for an Industrial Rectifier System. *Recent Adv. Electr. Electron. Eng.* **2014**, *7*, 65–74. [CrossRef]

26. Heathcote, M.J. *J & P Transformer Book*, 13th ed.; Reed Educational and Professional Publishing Ltd.: London, UK, 2003.